High- and low-temperature pyrolysis profiles describe volatile organic compound emissions from western US wildfire fuels

Kanako Sekimoto[1,2,3], Abigail Koss[1,2,4,*], Jessica B. Gilman[1], Vanessa Selimovic[5], Matthew M. Coggon[1,2], Kyle J. Zarzana[1,2], Bin Yuan[1,2,†], Brian M. Lerner[1,2,‡], Steven S. Brown[1,4], Carsten Warneke[1,2], Robert J. Yokelson[5], James M. Roberts[1], Joost de Gouw[1,2,4]

[1] NOAA Earth System Research Laboratory (ESRL), Chemical Sciences Division, Boulder, CO, USA

[2] Cooperative Institute for Research in Environmental Sciences, University of Colorado Boulder, Boulder, CO, USA

[3] Graduate School of Nanobioscience, Yokohama City University, Yokohama, Japan

[4] Department of Chemistry and Biochemistry, University of Colorado, Boulder, CO, USA

[5] Department of Chemistry, University of Montana, Missoula, MT, USA

[*] Now at Department of Civil & Environmental Engineering, Massachusetts Institute of Technology, Cambridge, MA, USA

[†] Now at Institute for Environment and Climate Research, Jinan University, Guangzhou, China

[‡] Now at Aerodyne Research, Inc., Billerica, MA, USA

Supporting Information

Contents

Table S1. (a) Data numbers and corresponding details of 15 different fuels used in PMF analysis. (b) Residuals of 2-factor PMF solutions. (c) Correlation of mass spectra of two factors between individual fuels and average of 15 fuels.

Fuel	(a) Data number for combined PMF				(b) Residual [%] [a]	(c) Correlation with average VOC emission profile (Figure 3)			
						High-temperature pyrolysis factor		Low-temperature pyrolysis factor	
	Total	Detail			Average ± STDV (maximum, minimum)	Slope	Correlation coefficient (*r*)	Slope	Correlation coefficient (*r*)
1. Ponderosa pine	10	Realistic	5	(Fire 01, 02, 37, 59, 72)	15.7 ± 7.6 (28.9, 7.7)	0.976 ± 0.004	0.9692	1.012 ± 0.005	0.9615
		Canopy	2	(Fire 19, 39)					
		Litter	1	(Fire 38)					
		Rotten log	2	(Fire 13, 73)					
2. Lodgepole pine	7	Realistic	4	(Fire 06, 07, 58, 63)	14.8 ± 4.9 (23.3, 10.9)	0.990 ± 0.004	0.9791	0.990 ± 0.002	0.9857
		Canopy	1	(Fire 40)					
		Litter	2	(Fire 21, 41)					
3. Loblolly pine	2	Litter	2	(Fire 35, 53)	6.3 ± 0.3 (6.6, 6.1)	0.989 ± 0.007	0.9307	0.960 ± 0.004	0.9414
4. Douglas fir	4	Realistic	2	(Fire 14, 57)	21.2 ± 9.3 (34.9, 14.9)	0.996 ± 0.004	0.9751	0.999 ± 0.003	0.9779
		Canopy	1	(Fire 18)					
		Litter	1	(Fire 43)					
5. Engelmann spruce	3	Realistic	1	(Fire 08)	20.5 ± 2.4 (22.2, 18.8) [b]	0.999 ± 0.006 [b]	0.9497 [b]	0.960 ± 0.004 [b]	0.9489 [b]
		Canopy	1	(Fire 25)					
		Duff	1	(Fire 26)	82.0 [c]	-	-	-	-
6. Subalpine fir	6	Realistic	2	(Fire 47, 67)	23.0 ± 14.1 (45.2, 9.1) [b]	1.001 ± 0.005 [b]	0.9674 [b]	0.999 ± 0.003 [b]	0.9771 [b]
		Canopy	2	(Fire 15, 23)					
		Litter	1	(Fire 51)					
		Duff	1	(Fire 56)	87.0 [c]	-	-	-	-
7. Juniper	2	Canopy	2	(Fire 68, 75)	6.4 ± 3.0 (8.5, 4.3)	1.016 ± 0.006	0.9419	0.971 ± 0.004	0.9492
8. Bear grass	1	-		(Fire 62)	5.6	1.039 ± 0.006	0.9406	1.006 ± 0.004	0.9578
9. Excelsior	2	-		(Fire 49, 61)	6.2 ± 3.0 (8.3, 4.0)	1.04 ± 0.01	0.8250	1.012 ± 0.007	0.9231
10. Ceatnothus	2	Shrub	2	(Fire 69, 74)	10.2 ± 1.1 (11.0, 9.5)	1.000 ± 0.007	0.9174	1.030 ± 0.006	0.9479
11. Chamise (contaminated)	3	Canopy	3	(Fire 24, 29, 46)	13.1 ± 3.9 (16.0, 8.6)	1.037 ± 0.006	0.9461	1.044 ± 0.004	0.9735
12. Chamise (uncontaminated)	3	Canopy	3	(Fire 27, 32, 48)	12.6 ± 2.0 (14.2, 10.4)	1.017 ± 0.005	0.9655	1.024 ± 0.004	0.9643
13. Manzanita (contaminated)	2	Canopy	2	(Fire 30, 33)	13.0 ± 1.1 (13.8, 12.3)	0.997 ± 0.004	0.9668	1.034 ± 0.004	0.9749
14. Manzanita (uncontaminated)	2	Canopy	2	(Fire 28, 34)	7.3 ± 1.1 (8.0, 6.5)	1.015 ± 0.005	0.9607	1.043 ± 0.005	0.9604
15. Sage	2	Shrub	2	(Fire 66, 71)	7.0 ± 2.1 (8.5, 5.6)	0.993 ± 0.005	0.9511	1.011 ± 0.004	0.9647

[a] Residual [%] = [Total measured ion signal - Total synthetic ion signal of high- and low-temperature factors] / Total measured ion signal x 100

[b] "Duff" data is excluded.

[c] The third factor has large fraction.

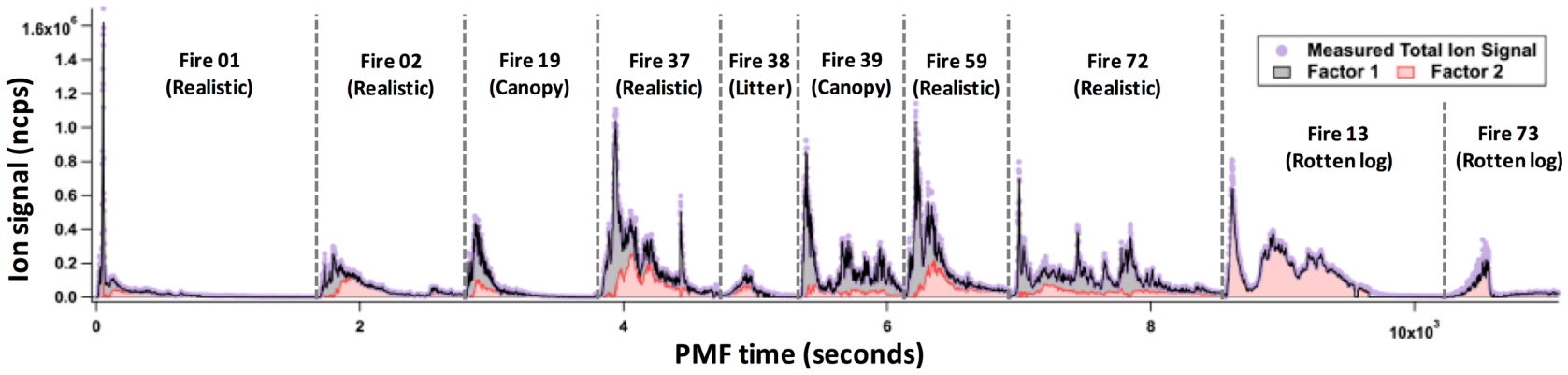

Figure S1. Time series of 2-factor PMF solution for Ponderosa pine dataset.

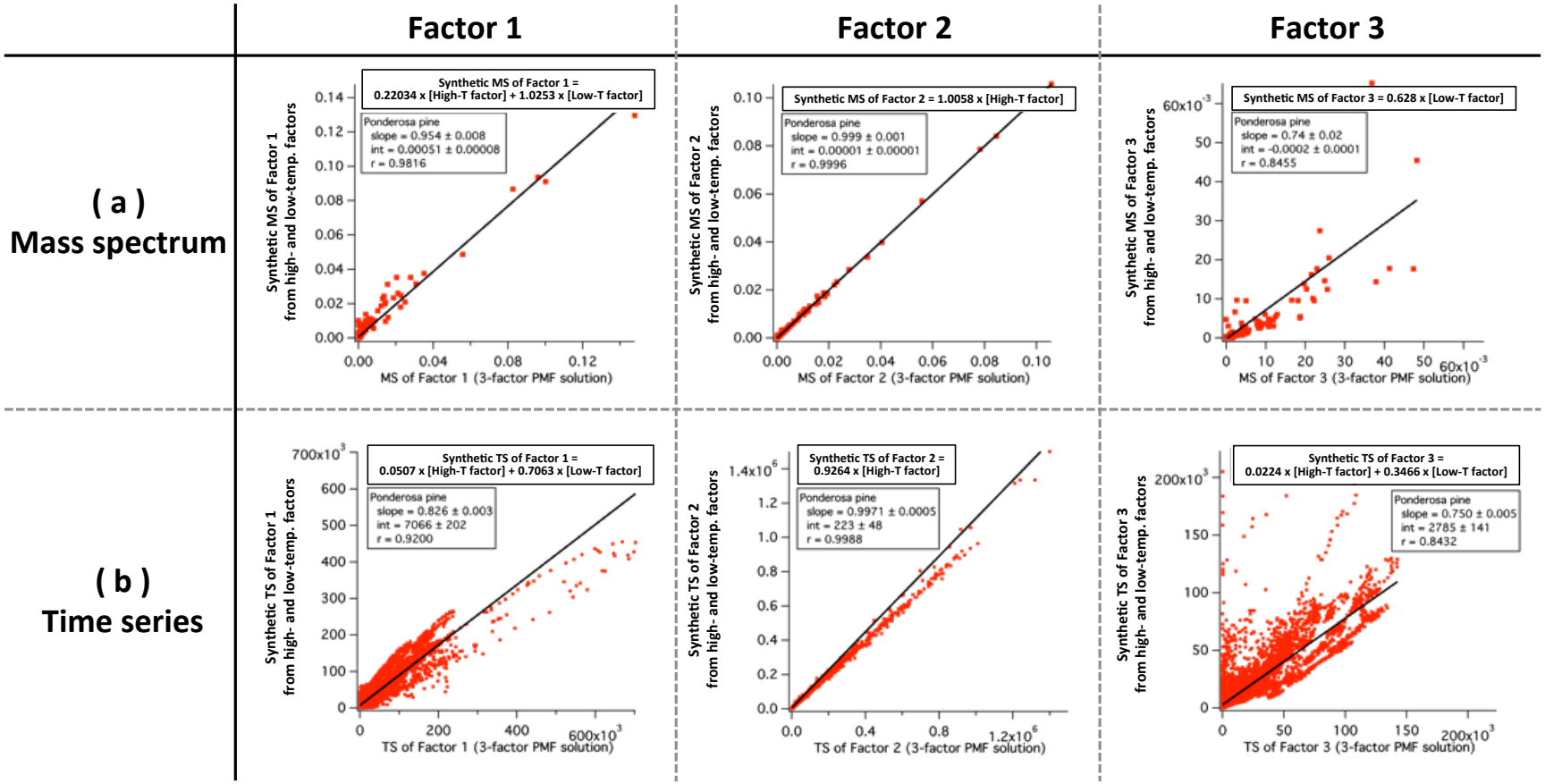

Figure S2. Comparison of 2-factor PMF solution (the high- and low-temperature pyrolysis factors discussed in main text) to a PMF solution with three factors. The individual factors from the 3-factor solution can be recreated with various linear combinations of the factors from the 2-factor solution (e.g., Factor 1 from 3-factor PMF solution = a×High-T factor + b×Low-T factor). The resulting synthetic 3-factor solution shown here is obtained from a linear best-fit of the high-/low-temperature factors to each of the original 3 factors. The comparison between the synthetic 3-factor solution reconstructed from linear combination of the high-/low-temperature factors, and the actual 3-factor solution directly derived from PMF is shown in (a) correlation of mass spectrum (ncps/total VOC ncps) and (b) time series (ncps) for Ponderosa pine datasets.

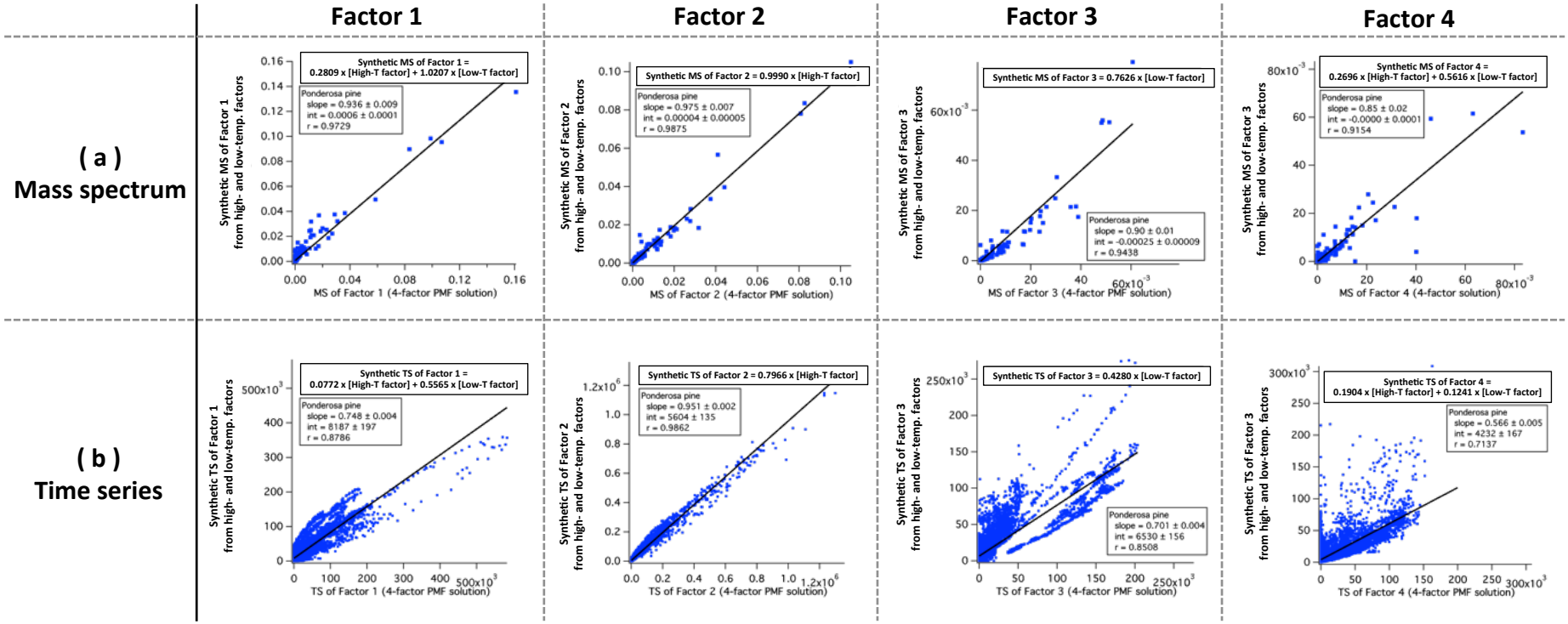

Figure S3. Comparison of 2-factor PMF solution (the high- and low-temperature pyrolysis factors discussed in main text) to a PMF solution with four factors. The individual factors from the 4-factor solution can be recreated with linear combinations of the factors from the 2-factor solution (e.g., Factor 1 from 4-factor PMF solution = a×High-T factor + b×Low-T factor). The resulting synthetic 4-solution shown here is obtained from a linear best-fit of the high-/low-temperature factors to each of the original 4 factors. The comparison between the synthetic 4-factor solution reconstructed from linear combination of the high-/low-temperature factors, and the actual 4-factor solution directly derived from PMF is shown in (a) correlation of mass spectrum (ncps/total VOC ncps) and (b) time series (ncps) for Ponderosa pine datasets.

Comparison of emission profile between each fuel and average (ncps/total VOC ncps)

(a) High-temperature pyrolysis factor

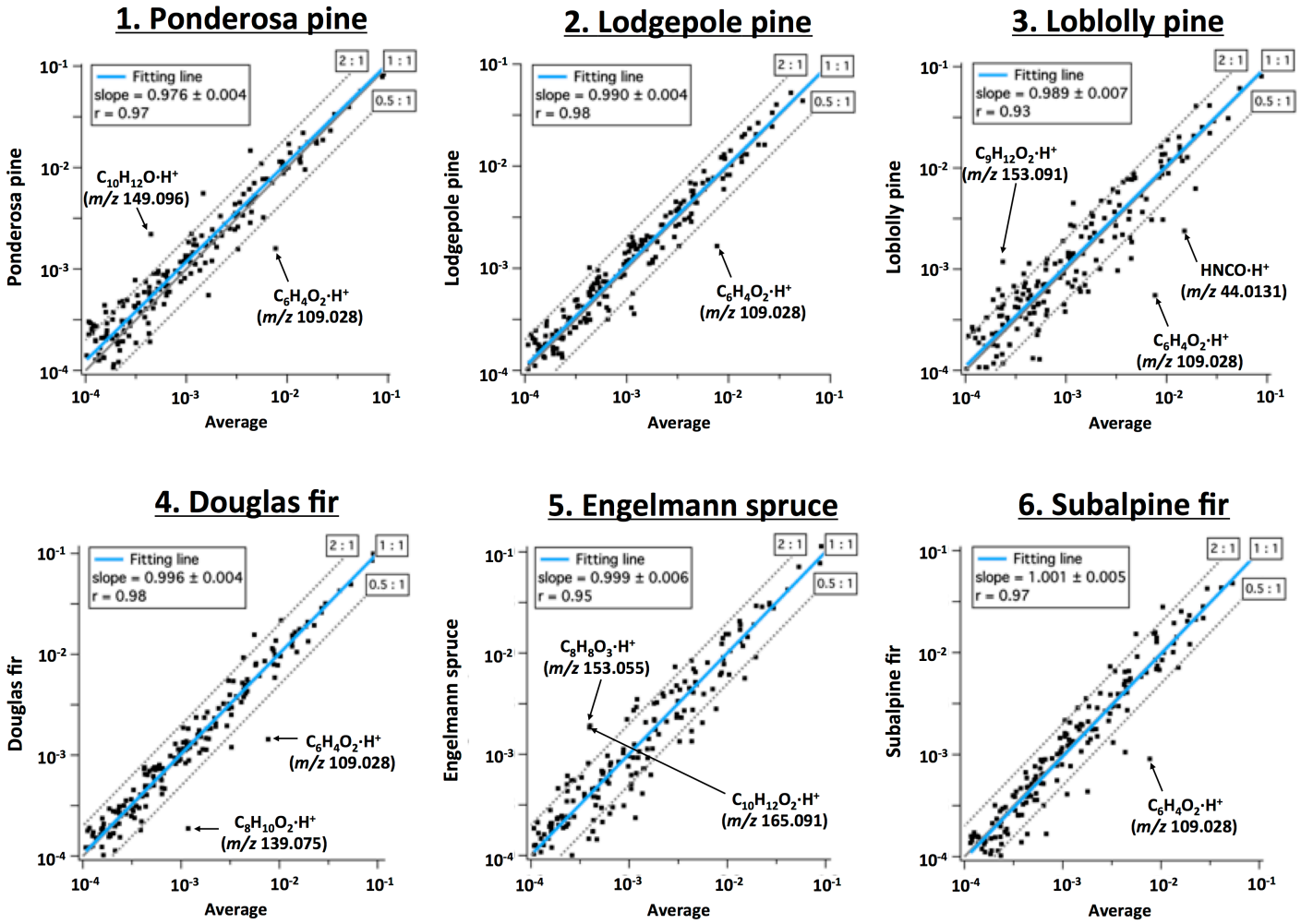

Figure S4. Comparison of (a) high- and (b) low-temperature pyrolysis VOC emission profiles (ncps/total VOC ncps) between each fuel and average of 15 different fuels shown in Figure 3.

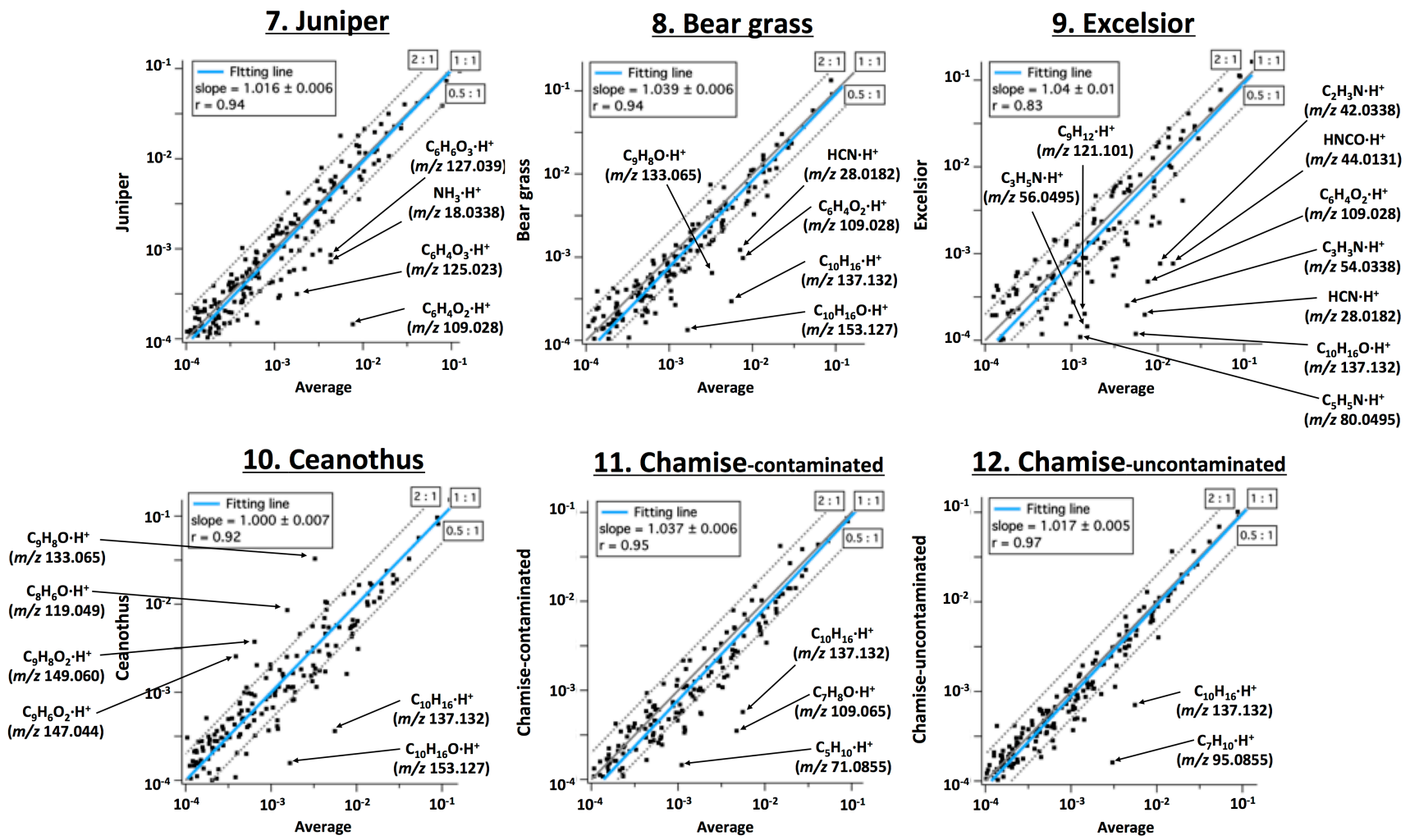

Figure S4. Continued.

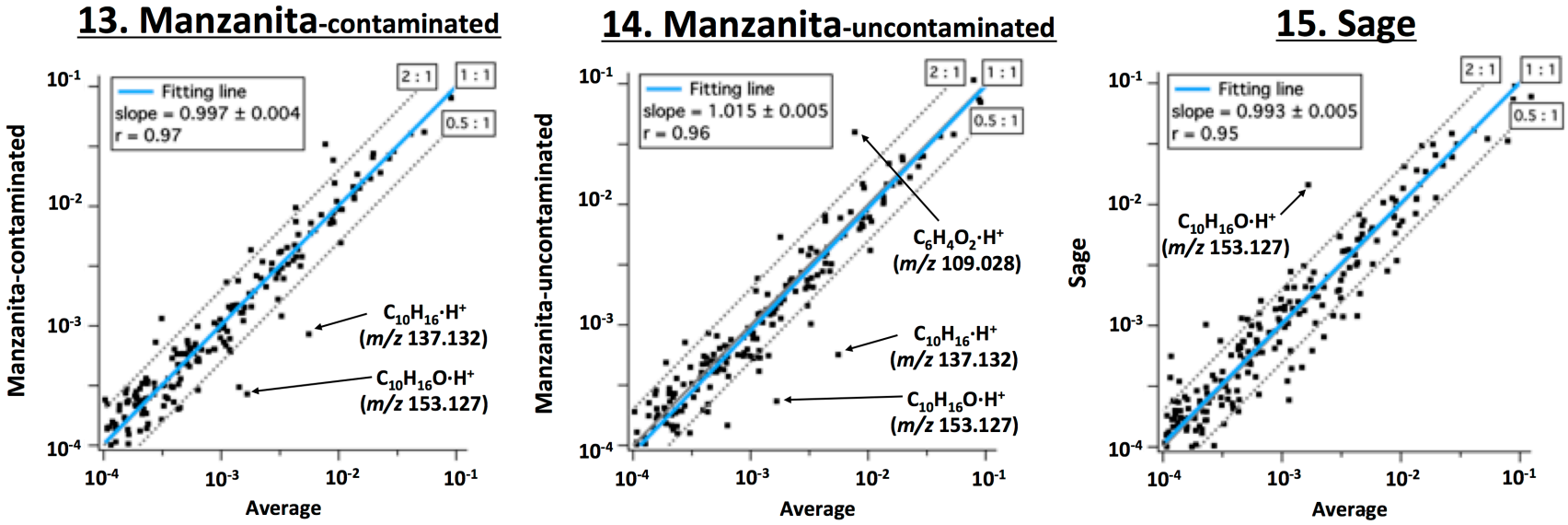

Figure S4. Continued.

(b) Low-temperature pyrolysis factor

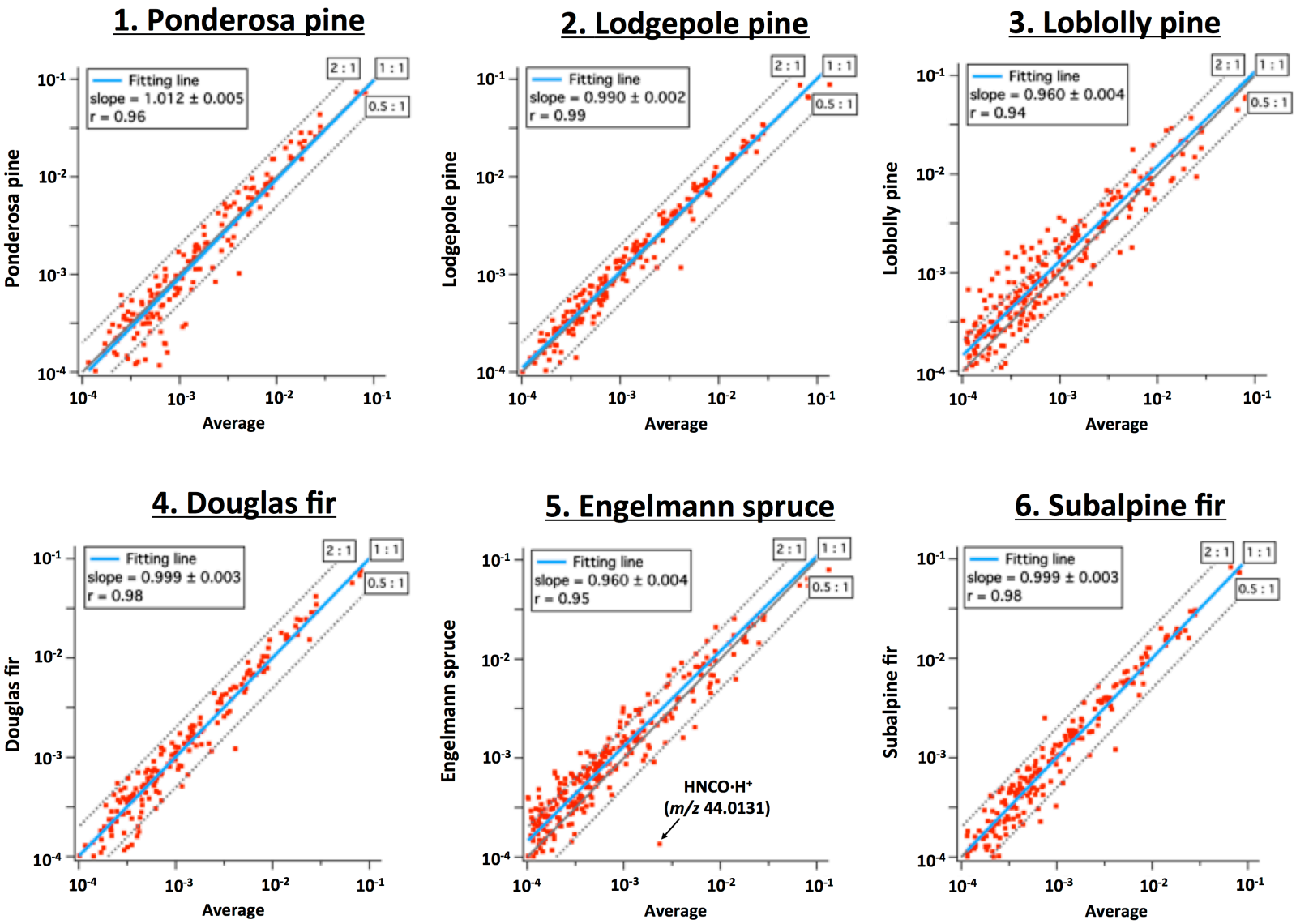

Figure S4. Continued.

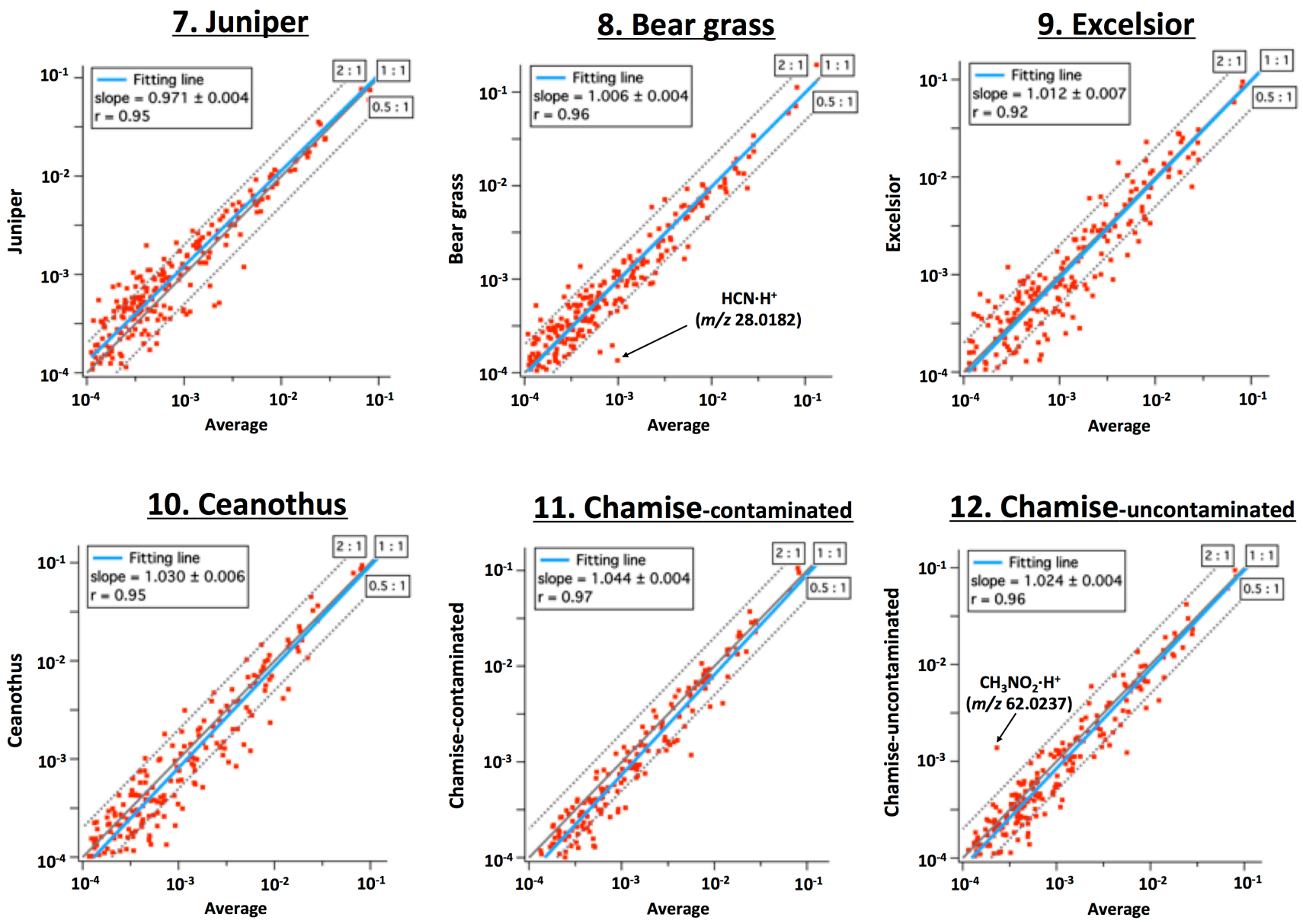

Figure S4. Continued.

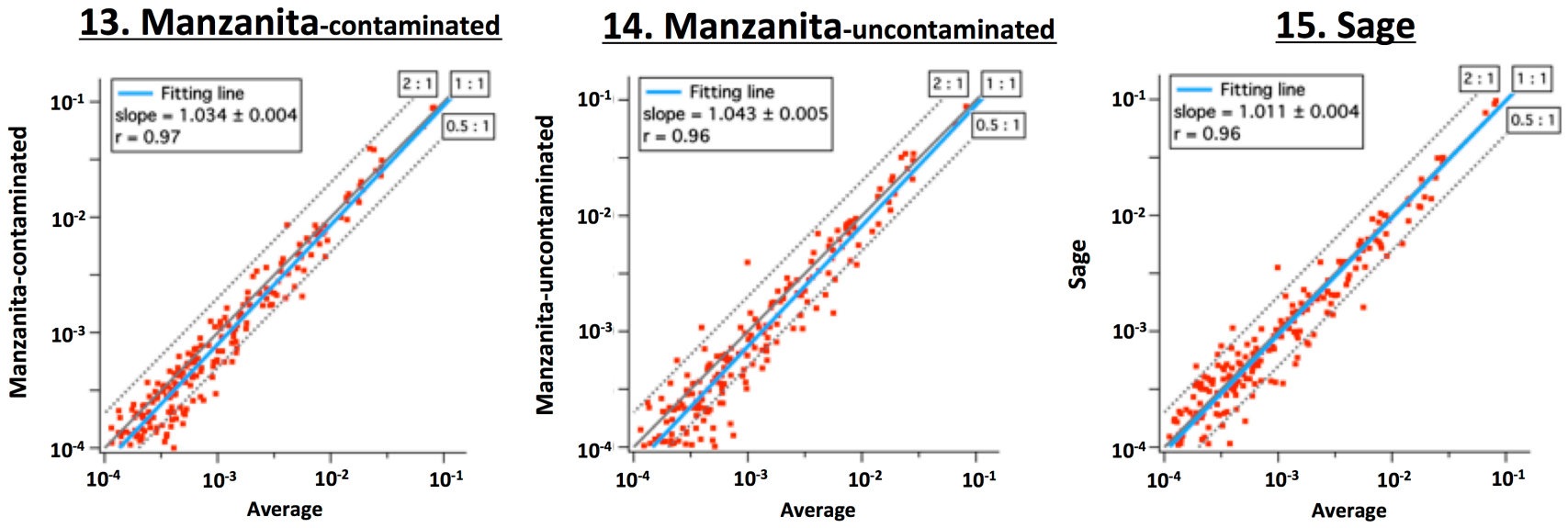

Figure S4. Continued.

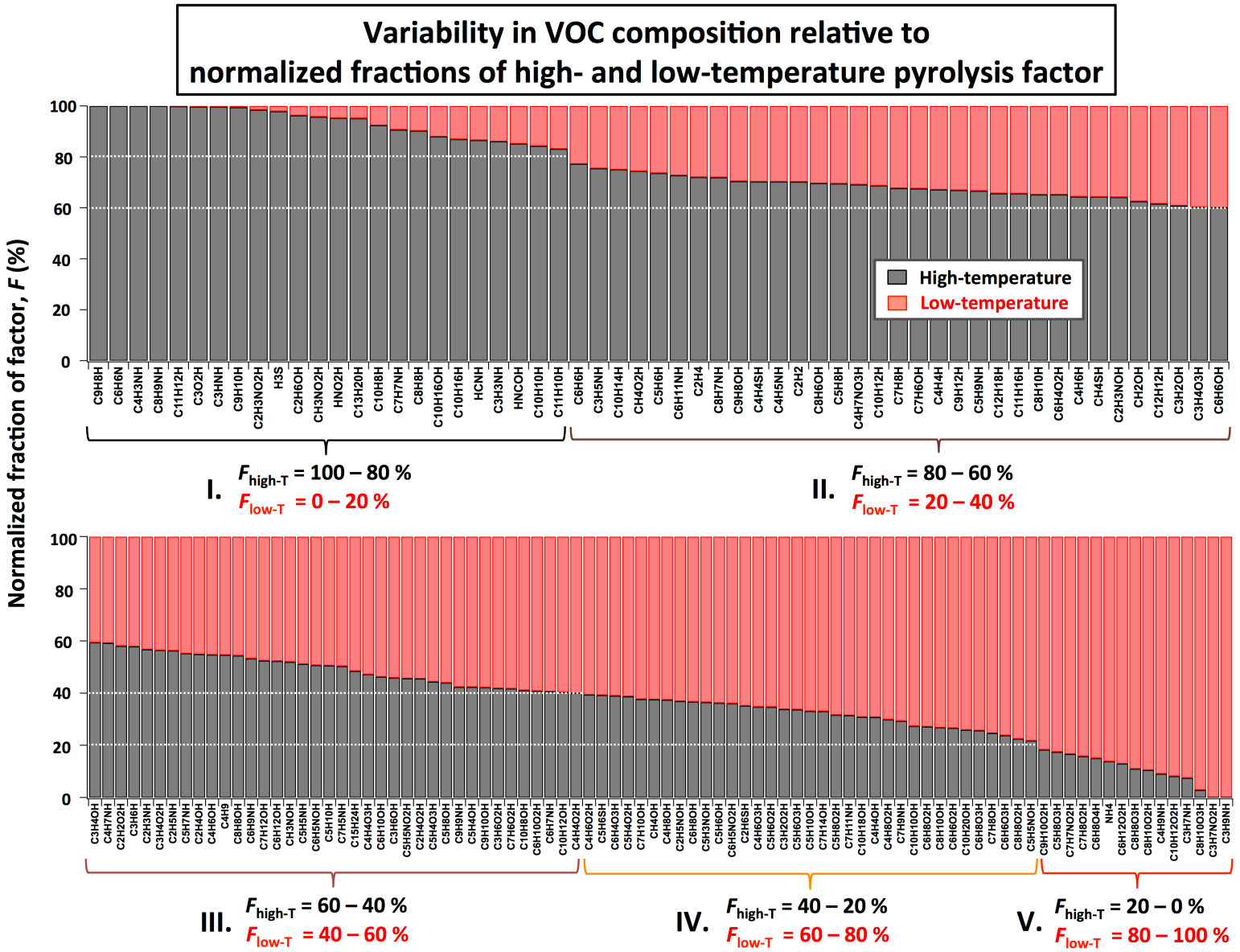

Figure S5. Variability in VOC composition relative to normalized fractions of the high- and low-temperature factors calculated from the average VOC profiles (Figure 3). The identified ion peaks were arranged in descending order of the normalized fraction of high-temperature factor.

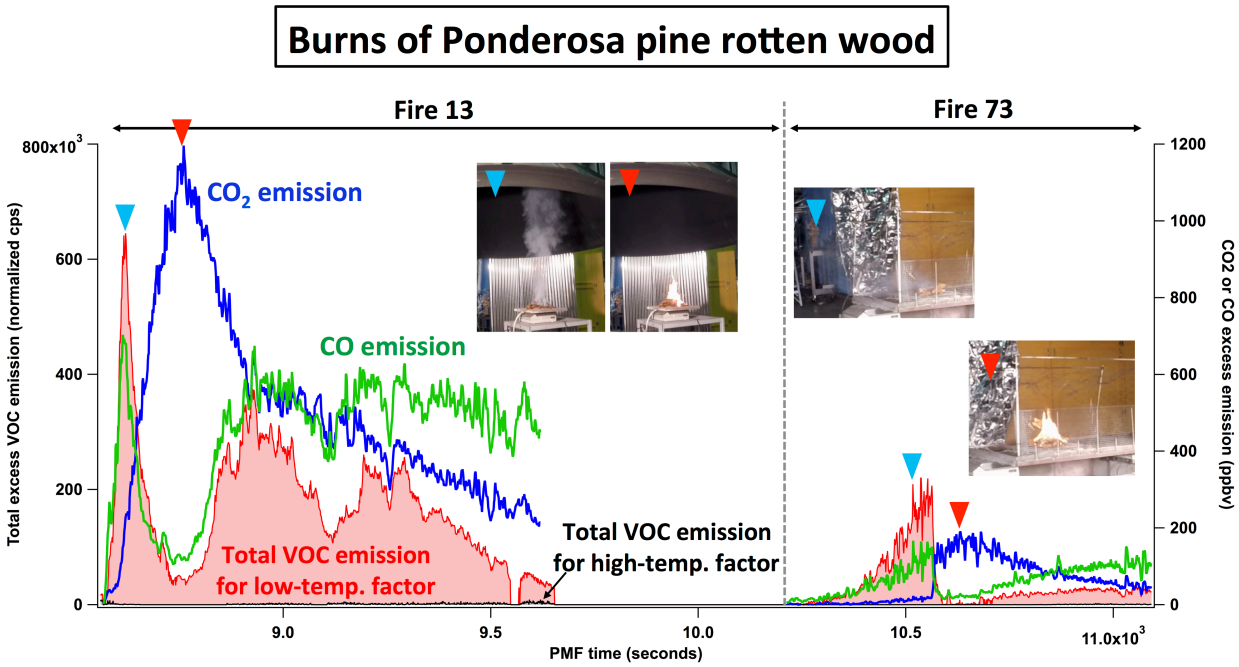

Figure S6. Results for burns of Ponderosa pine rotten wood (Fires #13 and #73).

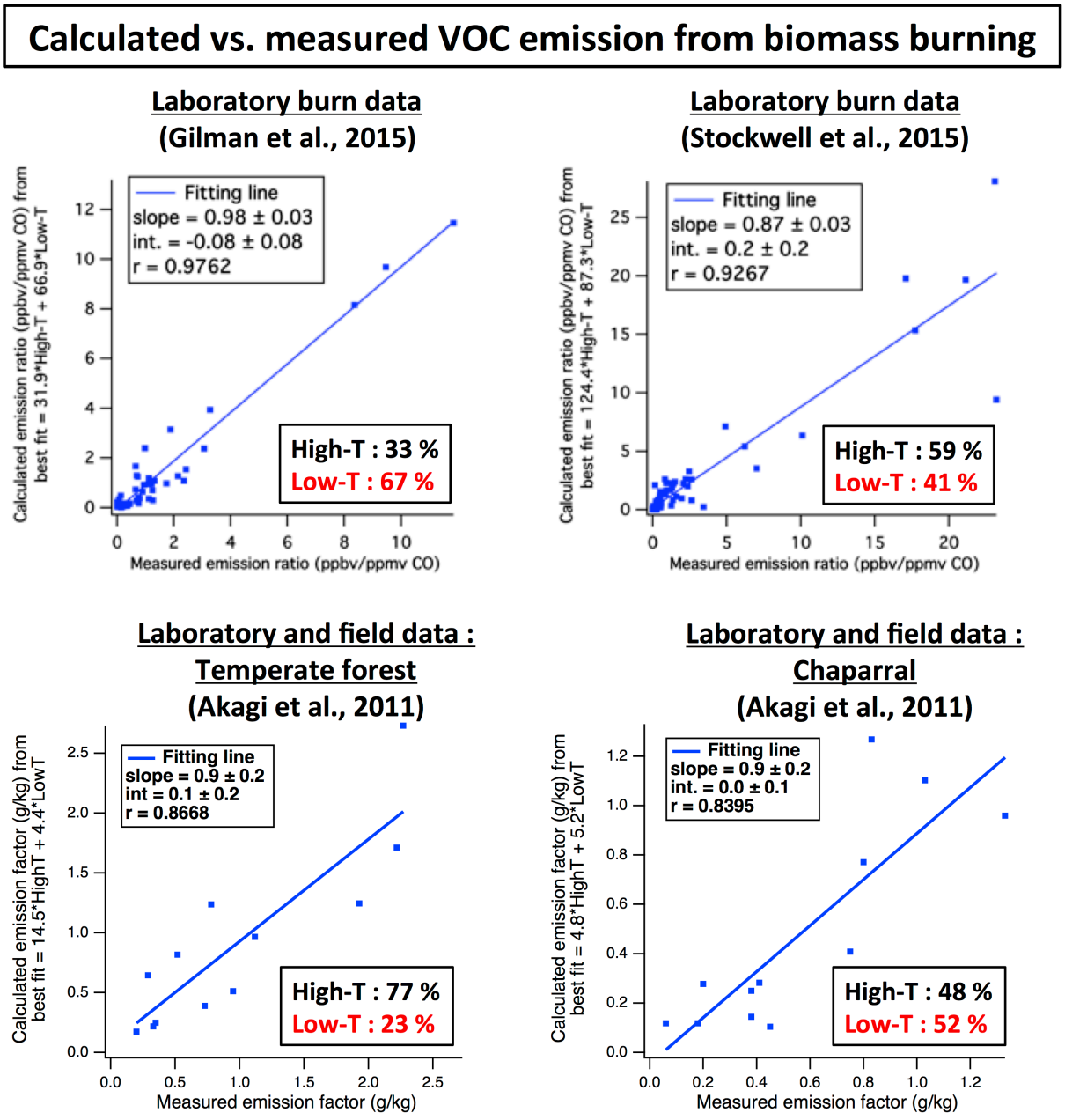

Figure S7. Scatter plots of calculated versus measured emissions for three literature data. Calculate emissions were obtained by fitting the VOC emission profiles (Figure 3). Laboratory study reported by Gilman et al. (2015) used fuels from southwestern, southeastern, and northern U.S. (e.g., pine, spruce, fir, chaparral, mesquite, and oak), while in the case of Stockwell et al. (2015), several types of grass, spruce, and chaparral were used.

§1. Preparation of datasets for PMF analysis

§1.1. Ion signal datasets

Ion signal datasets for PMF analysis were prepared using five steps. (i) 2 Hz time series data were averaged to 1 Hz. (ii) Background was subtracted from each ion signal before application of PMF, to avoid having PMF return a factor that describes the background. Background was determined from a 30-second to 5-minute measurement of combustion chamber air immediately prior to the fire. (iii) Points where instrument signal was negative or less than 0.01 were replaced with 0.01, which is based on the lowest limit of ion signal (ncps) of the PTR-ToF-MS. (iv) Data were restricted to the time period of active fire emissions, defined by the first enhancement of benzene above background (start) to when the PTR-ToF-CIMS stopped sampling (end). (v) The resulting time series for all fires of a particular fuel type (e.g., Ponderosa pine) were concatenated into a single data matrix.

§1.2. Uncertainty datasets

PMF also requires an estimate of measurement uncertainty of ion signals at each time point for each ion mass (*m/z*). The uncertainties ($\sigma_{m/z}$) were estimated as $\sigma_{m/z}\,(ncps) = 2.0 \times \sqrt{N_{m/z,w/o\ BG}\,(ncps)}$, where $N_{m/z,\ \mathrm{w/o\ BG}}$ is background-subtracted ion signal. The derivation is described below.

The uncertainty used in the present work is in units of "normalized counts-per-second (ncps)". The ncps uncertainty should have the same value relative to the ncps signal, as the uncertainty of the raw ion signal in units of counts-per-second (cps) relative to the cps signal. The raw ion signal (cps) is without normalization by the H_3O^+ ion intensities and correction for the ToF-duty cycle. The present uncertainty value ($\sigma_{m/z}$) for a given *m/z* ion signal ($N_{m/z}$) can be calculated as follows:

$$\sigma_{m/z}\,(ncps) = A \times \sqrt{N_{m/z}\,(ncps)} \times t \tag{S1-a}$$

$$A = \alpha_{m/z} \times \sqrt{\frac{10^6}{I_{H3O+}\,(cps)}} \times \sqrt{\frac{m/z_{reference}}{m/z}} \tag{S1-b}$$

A is a scaling factor of $\sqrt{N_{m/z}}$. $\alpha_{m/z}$ is a coefficient relative to the Poisson (counting) statistics ($\sigma = \sqrt{N}$) that accounts for additional noise to the ion signals of the masses due to the high-resolution peak fitting of the ToF mass spectra (Cubison et al., 2015; Corbin et al., 2015; Yuan et al., 2016). I_{H3O+} is the raw intensity of the H_3O^+ reagent ion, $m/z_{reference}$ is an arbitrary reference mass (in this work, $m/z_{reference}$ = 55), and t the sampling time (in this case, t = 1 s). The factors $10^6/I_{H3O+}$ and $\sqrt{m/z_{reference}/m/z}$ are to undo normalization by the H_3O^+ ion intensities and correction for the ToF-duty cycle, respectively.

Here we estimated a scaling factor $\alpha_{m/z}$ in Eq. (S1) suitable for the present instrumentation. Figure §1 shows standard deviations of the background signals (in units of cps) versus the background signals themselves from the individual zeroing periods for the 574 ion species listed in Table S2 during one burn (Fire #02). Most of data points are observed in the region between $\sqrt{N}$ and $3 \times \sqrt{N}$, suggesting that high-resolution peak fitting in this work can increase the errors in the ion signals by as much as a factor of 3 for the ion peaks. Figure §2 shows the empirically determined coefficient $\alpha_{m/z}$ (i.e., the ratio of standard deviation to $\sqrt{N}$) and scaling factor A (Eq. S1-b) for each m/z ion. It is seen that both the factors can be approximated as a constant (1.2 ± 0.4 and 0.6 ± 0.2, respectively), across a wide range of m/z. Accordingly, the empirical determined scaling factor A in Eq. (S1) can be approximated as 0.6, independent of the m/z value.

Based on the results described above, we first performed PMF using datasets of ion signals with backgrounds and uncertainties calculated from the empirical determined scaling factor A = 0.6 for single burn data (Fire #02, Ponderosa pine realistic mixture). The resulting 3-factor solution returned the high-temperature and low-temperature pyrolysis mass spectral and time series profiles as well as background profiles, but Q/Q_{exp} value was quite high (9.69 with fPeak and seed of zero). "Q" is a fit parameter of the PMF algorithm and is expressed by summation of squared scaled residuals for each experimental data points, i.e., $Q = \Sigma(\text{Resid}/\sigma)^2$ (Paatero, 1997; Ulbrich et al., 2009). Scaled residual (Resid/σ) at a certain data point is calculated as the ratio of residual (Resid) not fit by the PMF to uncertainty (σ) at that point. "Q_{exp}", expected Q, is associated with abs Resid/$\sigma \sim 1$. The value of $Q/Q_{exp} >> 1$ indicates underestimation of the uncertainties (Ulbrich et al., 2009). Thus, we performed several tests to see how sensitive the PMF results are to the uncertainty estimate, by setting A = 1.0, 1.5, 2.0, 2.5, and 3.0 and applying PMF. The profiles of the 3-factor solutions for individual uncertainty datasets were nearly

identical to the case of A = 0.6 (correlation coefficient > 0.99 as shown in Figure §3). Some small differences were seen in the quality of fit for ions with average enhancements of less than 10 ncps (corresponding to approximately 130 pptv and << 1% of total signal). These differences do not affect any of our conclusions. Interestingly, the Q/Q_{exp} value decreased with increasing the number of A: Q/Q_{exp} = 4.95, 2.65, 1.64, 1.12, and 0.78 for A = 1.0, 1.5, 2.0, 2.5, and 3.0, respectively (fPeak = seeds = 0, discussed in next section). Taking into account the Q/Q_{exp} value and the quality of fit, we decided A = 2.0 as the best number here.

Furthermore, we investigated changes to the PMF solution when using (i) the background-subtracted ion signals and (ii) concatenated burn data. If backgrounds are subtracted, or burns concatenated, the PMF results are quite similar to the base case obtained from the ion signals with backgrounds, A = 0.6, and single burn data (correlation coefficient r > 0.97 as shown in Figure §4). Consequently, the uncertainty datasets for concatenated burn data were prepared $\sigma_{m/z}\ (ncps) = 2.0 \times \sqrt{N_{m/z,w/o\ BG}\ (ncps)}$.

§1.3. Effect of rotational ambiguity (fPeak) and starting points (seeds) on PMF results

A subset of the rotational freedom of the 2-factor PMF solutions was explored by varying the fPeak values from -1.0 to +1.0, for the concatenated burn datasets consisting of the background-subtracted ion signals $N_{m/z,w/o\ BG}$ (ncps), and the uncertainty $\sigma_{m/z}\ (ncps) = 2.0 \times \sqrt{N_{m/z,w/o\ BG}\ (ncps)}$. In this study, solutions obtained from nonzero fPeak values (fPeak ≠ 0) were generally consistent with those from zero fPeak value (fPeak = 0). The resulting Q/Q_{exp} are almost constant (3.0292 ± 0.0003, as shown in Figure §5a). This means that the results shown in this work are associated to no rotation in the PMF analysis. In contrast, different random starting points (seeds = 0 – 10) were tried to find the local minimum of Q/Q_{exp} in the 2-factor PMF solutions (Paatero, 1997). The local minimum was obtained at seeds = 0 (Figure §5b). Therefore, the discussion in Section 3 in the main text is based on the 2-factor PMF solutions at fPeak = seeds = 0.

References

Cubison, M. J., and Jimenez, J. L.: Statistical precision of the intensities retrieved from constrained fitting of overlapping peaks in high-resolution mass spectra, Atmos. Meas. Tech., 8, 2333-2345, https://doi.org/10.5194/amt-8-2333-2015, 2015.

Corbin, J., Othman, A., Allan, D. J., Worsnop, R. D., Haskins, D. J., Sierau, B., Lohmann, U., and Mensah, A. A.: Peak-fitting and integration imprecision in the Aerodyne aerosol mass spectrometer: effects of mass accuracy on location- constrained fits, Atmos. Meas. Tech., 8, 4615-4636, https://doi.org/10.5194/amt-8-4615-2015, 2015.

Paatero, P.: Least squares formulation of robust non-negative factor analysis, Chemometr. Intell. Lab., 37 (1), 23-35, https://doi.org/10.1016/S0169-7439(96)00044-5, 1997.

Ulbrich, I. M., Canagaratna, M. R., Zhang, Q., Worsnop, D. R., and Jimenez, J. L.: Interpretation of organic components from Positive Matrix Factorization of aerosol mass spectrometric data, Amos. Chem. Phys., 9 (9), 2891-2918, http://doi.org/10.5194/acp-9-2891-2009, 2009.

Yuan, B., Koss, A., Warneke, C., Gilman, J. B., Lerner, B. M., Stark, H., and de Gouw, J. A.: A high resolution time-of-flight chemical ionization mass spectrometer utilizing hydronium ions (H_3O^+ ToF-CIMS) for measurements of volatile organic compounds in the atmosphere, Atmos. Meas. Tech., 9 (6), 2735-2752, http://doi.org/10.5194/amt-9-2735-2016, 2016.

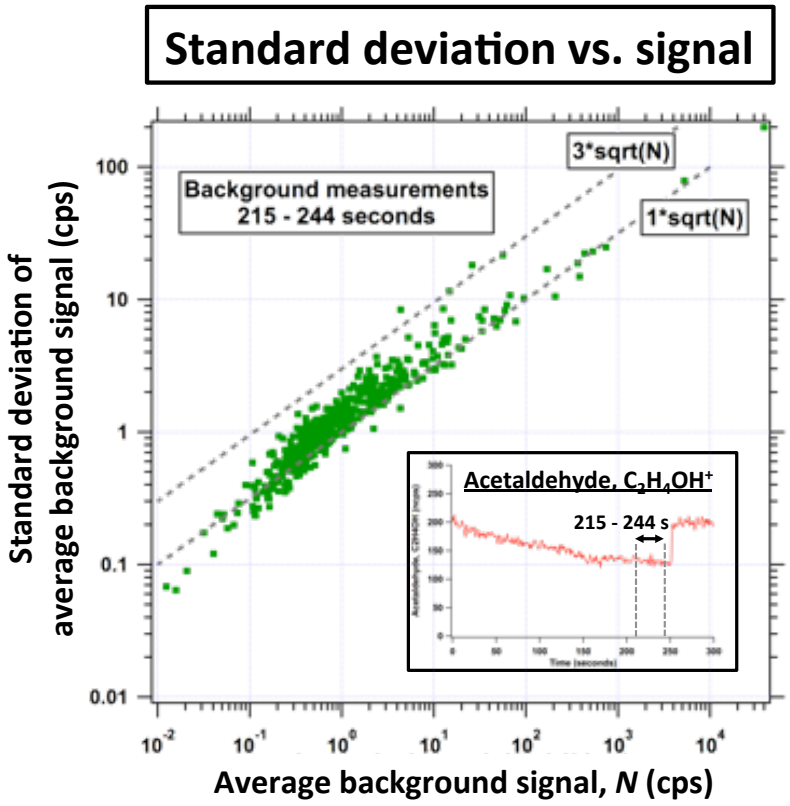

Figure §1. Scatterplot of the standard deviations of background signals versus the measured background signals from Fire #02 for 574 ion peaks which were used for PMF analysis. In this graph, the signals are not corrected for the H_3O^+ ion intensities and the ToF duty cycle. The two dashed lines are $\sqrt{N}$ and $3 \times \sqrt{N}$, respectively.

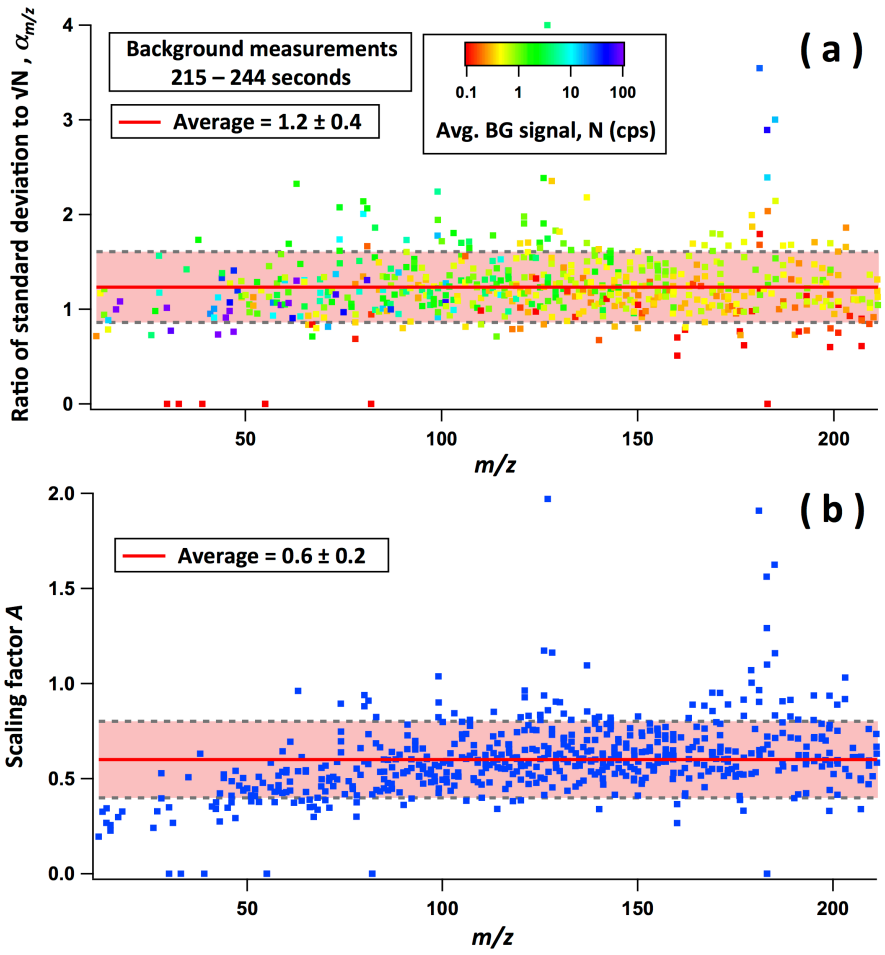

Figure §2. Scatterplots of (a) ratio of standard deviation to background signals ($\alpha_{m/z}$) and (b) scaling factor A versus the m/z values. The coefficient $\alpha_{m/z}$ was obtained from the data shown in Figure §1. The scaling factor A was determined from Eq. S1-b and the average $\alpha_{m/z}$ value of 1.2.

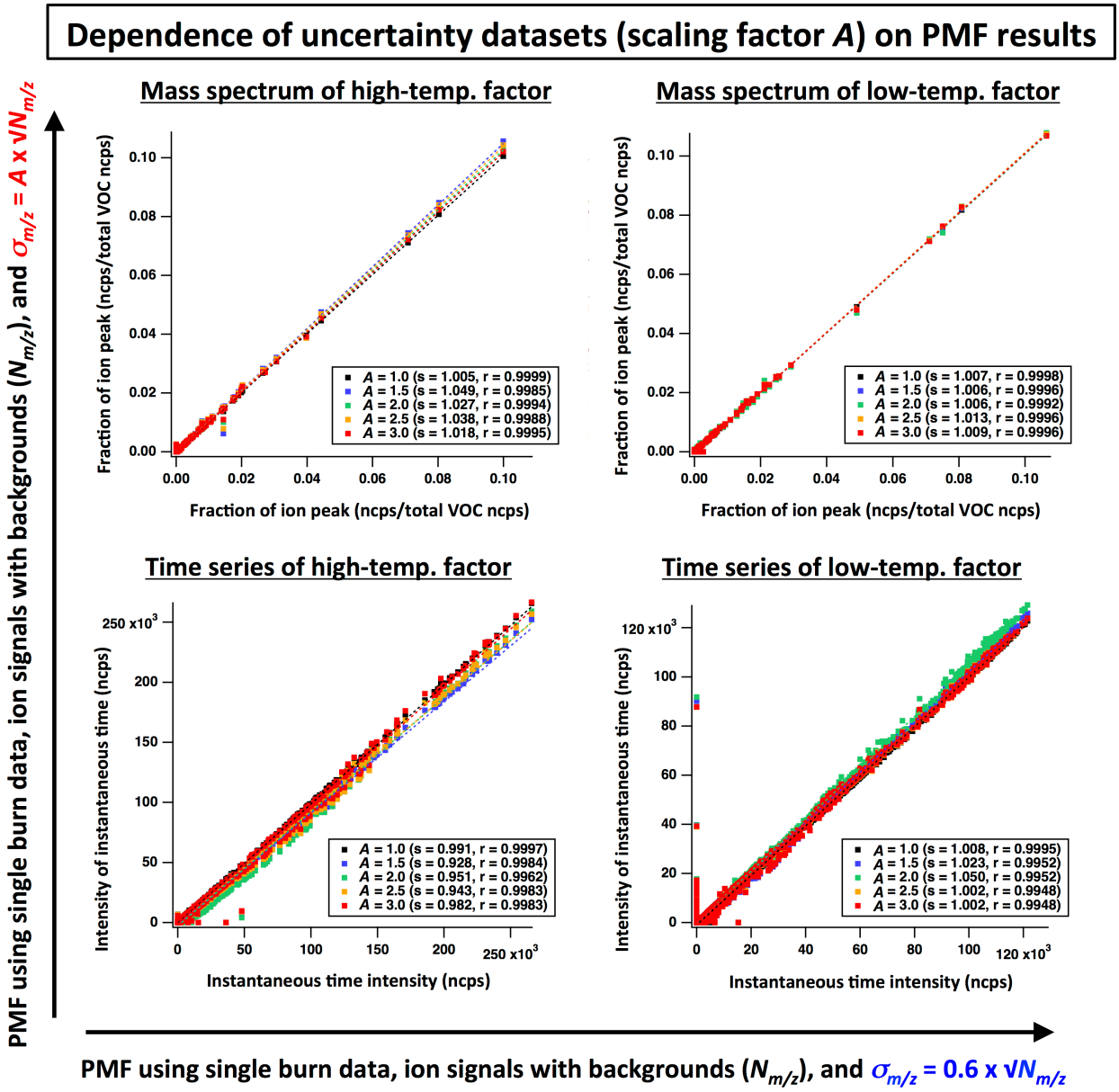

Figure §3. Dependence of uncertainty datasets, scaling factor *A* in Eq. (S1), on PMF results (mass spectra and time series for high- and low-temperature pyrolysis factors at fPeak = seeds = 0). The PMF results obtained from scaling factor *A* = 1.0, 1.5, 2.0, 2.5, and 3.0 are compared with the results from *A* = 0.6. Single fire data (Fire #02, Ponderosa pine realistic mixture) and ion signals with backgrounds are used. "s" and "r" in each panel represent the slope and correlation coefficient for the linear line of the best fit, respectively.

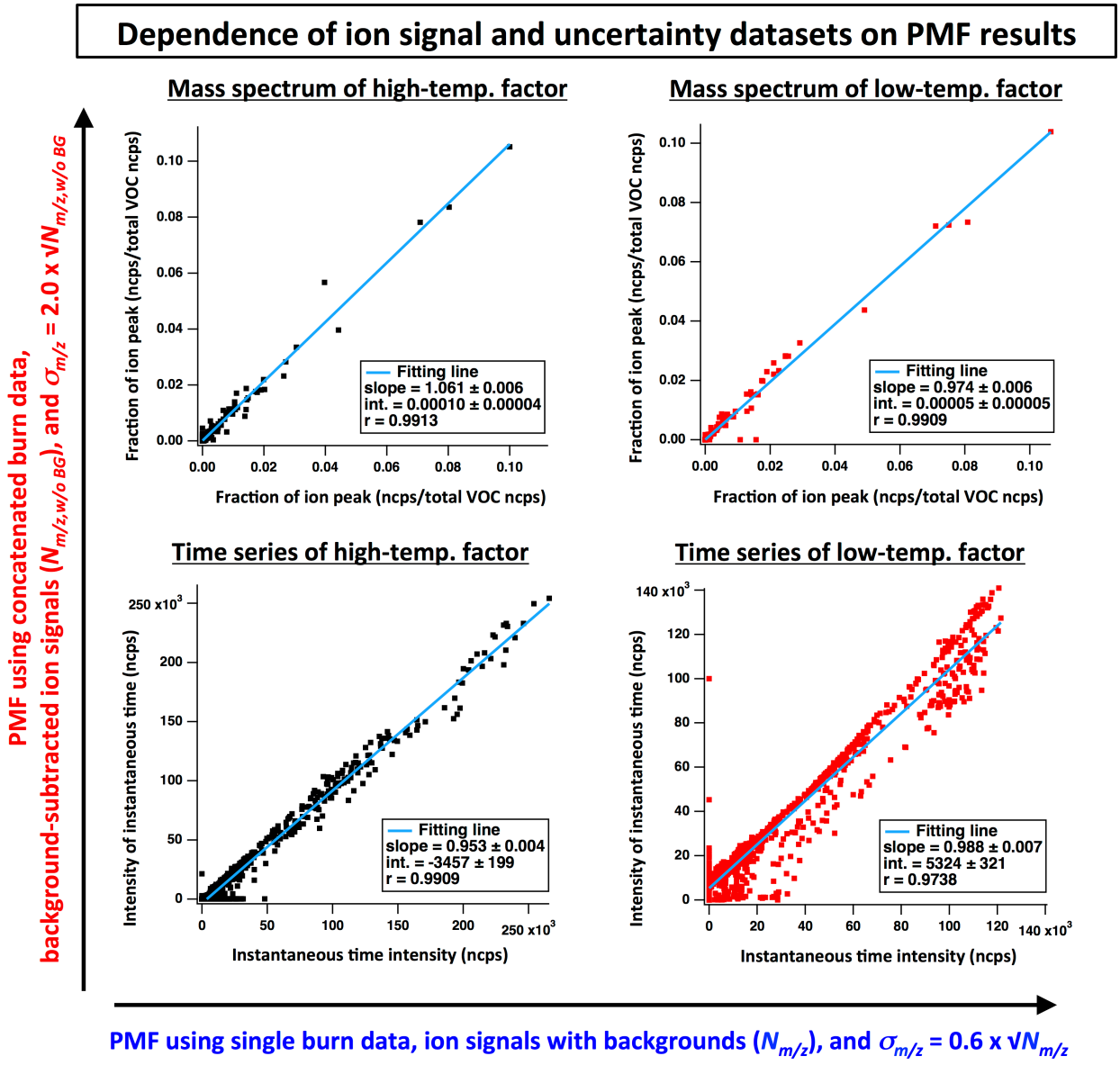

Figure §4. Dependence of ion signal and uncertainty datasets on PMF results (mass spectra and time series for high- and low-temperature pyrolysis factors at fPeak = seeds = 0). The PMF results obtained from concatenated burn data (10 Ponderosa pine burn data), background-subtracted ion signals, and the scaling factor A = 2.0 in Eq. (S1) are compared with the results from single burn data (Fire #02, Ponderosa pine realistic mixture), ion signals with backgrounds, and A = 0.6.

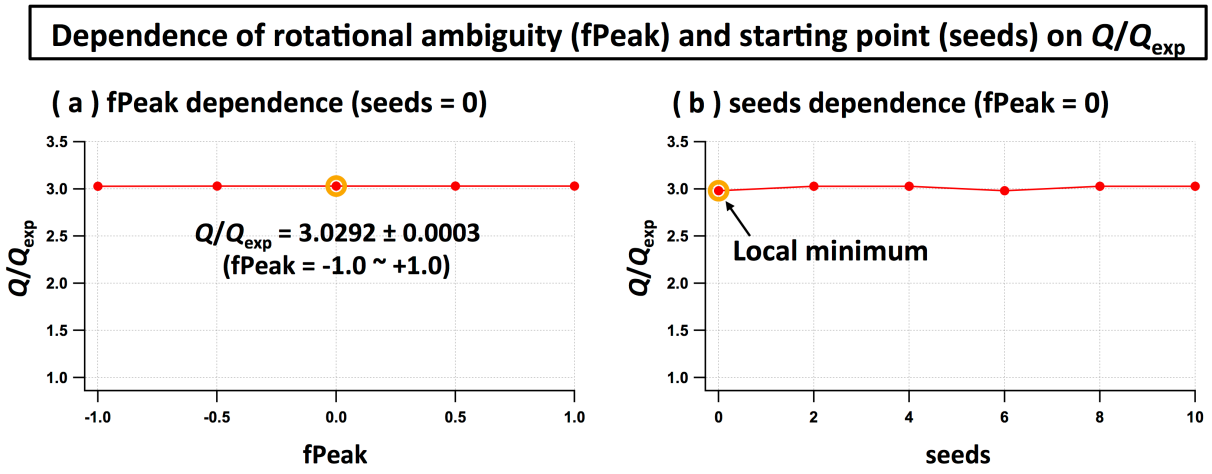

Figure §5. Dependence of rotational ambiguity (fPeak) and starting point (seeds) on Q/Q_{exp} for the 2-factor PMF solutions of the concatenated Ponderosa pine burn datasets. These datasets consist of the background-subtracted ion signals $N_{m/z,w/o\ BG}$ (ncps), and the uncertainty $\sigma_{m/z}\ (ncps) = 2.0 \times \sqrt{N_{m/z,w/o\ BG}\ (ncps)}$.